An New View on the Evolution of Seawater Molybdenum Inventories before and during the Cretaceous Oceanic Anoxic Event 2

Christopher Siebert[1]*, Florian Scholz[1], Wolfgang Kuhnt[2]

[1]GEOMAR Helmholtz Centre for Ocean Research Kiel, Wischhofstraße 1-3, 24111 Kiel, Germany

[2]Marine Micropaleontology, Institute of Geoscience, University of Kiel, Ludewig-Meyn-Straße 14, 24118 Kiel, Germany

**corresponding author: csiebert@geomar.de*

ABSTRACT

Extreme periods of global warming in Earth's history have been strongly associated with declining oxygen concentrations in the ocean, a scenario not unlike the current evolution of ocean oxygenation. One of the most intense Phanerozoic deoxygenation events (so called Ocean Anoxic Events (OAE)) is the late Cretaceous OAE2 approximately 94Ma ago. Although several studies have investigated the evolution of redox sensitive proxies during the OAE2 event, geochemical records that span the time period leading up to OAE2, in particular for molybdenum (Mo) and its isotopes are rare. Here, we investigate Mo cycling in the Tarfaya upwelling system in the Cretaceous proto-North Atlantic before and during Oceanic Anoxic Event (OAE) 2 throughout a 5 Ma record. The observed changes in sedimentary Mo isotope compositions can be explained by a mode of Mo cycling similar to that in modern oxygen minimum zones. Based on this interpretation we estimate the pre-OAE2 Mo isotope composition of seawater to be 1.6‰ indicating that late Cretaceous pre-OAE2 seawater had a lighter Mo isotope composition than the modern ocean. We suggest that Mo burial in oxic sediments was likely diminished under conditions of globally reduced oxygen concentrations. This allows us to model the Mo isotope composition of late Cretaceous pre-OAE2 seawater without lowering of the seawater

Mo inventory (e.g., -55 % oxic sink, + 40 % anoxic sink). Previous estimations of the Mo seawater isotope composition during OAE2 are close to the signal observed pre-OAE here. The Mo isotope variation associated with the onset of OAE2 is therefore small, which is unexpected because strong expansion of anoxic sedimentation in OAE2 is indicated by e.g. sulfur isotopes. A further decrease of Mn burial rates in the open ocean during OAE2 could "buffer" the Mo seawater isotope signal during OAE2, to account for this small offset. Our findings emphasize that changes to the relative size of not only the anoxic sink but also the oxic sink are important considerations when interpreting paleo-Mo isotope data.

Keywords: Cretaceous, Ocean Anoxic Event (OAE), molybdenum isotopes, Mo/TOC, Oxygen Minimum Zone (OMZ), anoxic

1. INTRODUCTION

The current "Anthropocene" trend of declining oxygen concentrations in the ocean (e.g., Schmidtko et al., 2017) has led to increased scientific interest in the causal, spatial and temporal dynamics of ocean deoxygenation events in Earth's history. These events were usually associated with the release of large volumes of carbon dioxide into the Earth's atmosphere, for example via eruption and emplacement of large igneous provinces, causing subsequent periods of global warming (e.g. Arthur et al., 1985). The resulting greenhouse conditions cause, among other things, enhanced continental chemical weathering and increased nutrient supply to the ocean supporting increased primary production and oxygen depletion. In addition, changing hydrographic conditions due to warming ocean water result in reduced ocean ventilation and can amplify the effect of ocean deoxygenation.

One of the most intense deoxygenation events (so called Ocean Anoxic Event (OAE)) is the Cretaceous OAE2 or "Bonarelli" event at the Cenomanian-Turonian Boundary approximately 94Ma ago (e.g. Jenkyns, 2010; Friedrich et al., 2012). OAE2 is marked by a global positive carbon isotope excursion

(CIE) due to worldwide increased deposition of organic carbon under reducing conditions and subsequent burial of organic rich sediments in particular in the proto-North Atlantic region (e.g. Kuypers et al., 2004; Kolonic et al., 2005, Owens et al., 2018).

In order to constrain timing and causalities of these global deoxygenation events, enrichment factors of redox sensitive trace elements in reducing sediments are often used to unravel the local and global oxygenation history (e.g. Crusius et al., 1996; Morford & Emerson, 1999; Algeo & Lyons, 2006; Tribovillard et al., 2006). Stable isotope fractionation of some of these redox sensitive trace elements under various redox conditions has become a focus of investigation in order to better understand the processes involved in their sedimentary enrichment and in order to attempt quantification of the extent of reducing conditions.

In particular molybdenum (Mo) and its stable isotopes (reported as $\delta^{98}Mo = ((^{98}Mo/^{95}Mo)_{sample}/(^{98}Mo/^{95}Mo)_{NIST3134} - 1) \cdot 1000$) have been used to reconstruct the global extent of seafloor area that was covered by anoxic and sulfidic (euxinic) bottom water in the geological past (e.g., Arnold et al., 2004; Pearce et al., 2008; Dickson et al., 2017). This approach is based on the modern ocean's Mo mass balance. The uniform concentration (~105 nmol kg^{-1} with a seawater residence time of approximately 400ka (Miller et al., 2011) and isotope composition ($\delta^{98}Mo_{seawater}$ = +2.05 ‰) (Siebert et al., 2003; Nakagawa et al., 2012) of Mo in seawater are controlled by the balance between Mo input via continental runoff ($\delta^{98}Mo_{input}$ = +0.4 ‰) (e.g. Archer & Vance, 2008) on one side and burial of isotopically light Mo with manganese (Mn) oxide minerals in oxic sediments ($\Delta^{98}Mo_{seawater-sediment}$ = ~2.85 ‰) (Barling et al., 2001; Siebert et al., 2003) and organic material or sulfide minerals in anoxic sediments ($\Delta^{98}Mo_{seawater-sediment}$ = ~0.8‰) (Poulson-Brucker et al., 2009) on the other side. Early in the history of the Mo isotope proxy, it was found that the $\delta^{98}Mo$ of sediments in the highly restricted and euxinic Black Sea basin mirrors the $\delta^{98}Mo$ of seawater due to highly efficient Mo removal (e.g., Arnold et al., 2004, Neubert et al., 2008). Based on the assumption that under certain conditions sediments underneath euxinic waters record the $\delta^{98}Mo$ of contemporary seawater, these sediments were investigated as archives for changes in the Mo isotope composition of global seawater and

75 therefore in the global Mo isotope balance reflecting the extent of anoxic versus oxic sedimentation
76 during specific periods in Earth's history.

77 Another proxy tool often used to evaluate redox conditions and authigenic Mo enrichment from
78 seawater at the basin scale are ratios of Mo to total organic carbon (TOC) (e.g. Algeo and Lyons, 2006).
79 Mo and TOC are both enriched in euxinic environments and changes in their ratio have been used to
80 make qualitative statements about changes in the (local or global) dissolved Mo reservoir (e.g.
81 Tribovillard et al., 2006, Scott and Lyons 2012). In modern euxinic basins sedimentary Mo/TOC
82 generally decreases with increasing degree of basin restriction and decreasing deep water Mo
83 concentration. Specifically, euxinic basins with sluggish deep-water renewal (e.g., Black Sea) are
84 characterized by Mo-depletion in the deep-water (normalized to salinity) and lower sedimentary
85 Mo/TOC than euxinic basins with frequent deep-water renewal (e.g., Cariaco Basin).

86 However, in order to evaluate and interpret the proxies described above in a more quantitative way,
87 the overall redox conditions at the investigated sites have to be constrained independently, which is
88 often approached using iron (Fe) speciation analysis. This proxy is based on the extend of sedimentary
89 enrichment of highly reactive Fe (Fe_{HR}: biogeochemically available Fe) in relation to total Fe (Fe_T). A
90 ratio of Fe_{HR} to Fe_T higher than 0.38 is commonly interpreted as evidence for anoxic depositional
91 conditions in general (see e.g. Poulton and Canfield, 2011 for details). Sediments with a Fe_{HR}/Fe_T
92 indicative of anoxia can be further classified using the "Extent of Pyritization" of the highly reactive Fe
93 pool (expressed as Fe_{Py}/Fe_{HR}) where values <0.7 are thought to indicate ferruginous conditions Fe >
94 H_2S in the water column), whereas values >0.7 are thought to indicate euxinic (free H_2S_{aq} in the water
95 column) depositional conditions.

96 Based on the proxies discussed above, numerous studies have inferred a local and global depletion of
97 the seawater Mo reservoir during OAE2 and presented estimates on global anoxia (e.g., Owens et al.,
98 2013; Poulton et al., 2015; Dickson et al., 2016; Goldberg et al., 2016; Owens et al., 2016; Dickson et
99 al., 2021) These and other studies also show that it is often difficult to differentiate between a local
100 and a global signal when applying these proxies to a paleo-setting.

Recent research findings in modern more open-marine anoxic environments, indicate that the use of these proxies for ocean redox changes in paleo-settings have to be evaluated carefully (e.g. Hardisty et al., 2018; Scholz, 2018; Raiswell et al., 2018; Kendall et al., 2020). In terms of Mo isotope compositions, the Black Sea is virtually the only euxinic basin where sedimentary δ^{98}Mo reflects δ^{98}Mo of seawater. In addition, Helz et al. (2011) suggested that a highly efficient Mo removal under euxinic conditions does not only depend on the concentration of free H_2S in the water column (>11uM H_2S_{aq}, e.g. Zheng et al., 2000), but also on pH and dissolved Fe availability. Euxinic basins with more frequent deep-water renewal typically display a Mo isotopic offset between sediment and seawater, which implies partial removal of a fractionated Mo pool (Arnold et al., 2004; Neubert et al., 2008; Noordmann et al., 2015; Scholz et al., 2018; Brüske et al., 2020). Sedimentary δ^{98}Mo values observed in these partially restricted basins are, on average, similar to values in open-marine oxygen-depleted systems (in particular upwelling-related oxygen minimum zones, OMZs), where hydrogen sulfide is limited to the sediment pore water most of the time (δ^{98}Mo = ~1.5 ‰) (Poulson-Brucker et al., 2009; Scholz et al., 2017; Eroglu et al., 2020). The mechanisms of Mo isotope fractionation in weakly restricted euxinic basins and open-marine OMZs are a matter of ongoing debate. Scavenging of dissolved Mo by manganese (Mn) or Fe oxy-(hydroxides) in the water column, formation of intermediate thiomolybdate species and interactions between Mo, H_2S and organic matter, both above and below the sediment-water interface, are likely to play an important role (Neubert et al., 2008; Helz et al., 2011; Dahl et al., 2017; Scholz et al., 2017, 2018). The important point here is that sedimentary δ^{98}Mo values resulting from partial removal of a fractionated Mo pool are difficult to discern from δ^{98}Mo values that reflect a globally depleted Mo reservoir in a paleo-setting. Furthermore, sediments in open-marine (and thus Mo-replete) anoxic systems are also characterized by low Mo/TOC without having to be euxinic (Algeo and Lyons, 2006). Furthermore, there is increasing evidence that the interpretation of Fe speciation in deep time is not as straightforward as previously assumed and that for example a ferruginous signature can be produced by different sets of environmental variables (Scholz, 2018, Scholz et al., 2019a, b).

In this study we focus strongly on the paleo-setting of our sample site and compare Mo isotope and Mo/TOC data for the Tarfaya upwelling system in the late Cretaceous Proto-North Atlantic with those from the present-day Peruvian OMZ as a modern-day equivalent. We will show that seawater Mo isotope compositions were lower pre-OAE2 than modern day seawater isotope ratios and present a model by which these isotope compositions can be explained without coeval drawdown of the Mo reservoir. We further put forth a scenario where fluctuation of oxygen minimum zone (OMZ) boundaries rather than Mo depletion in the water column can explain the Mo proxy signatures observed in Tarfaya across OAE2. The presented ideas are not necessarily intended to replace existing models for Cretaceous seawater evolution, however, we would like to demonstrate that a detailed understanding of modern day equivalents of ancient settings can help the development of alternative scenarios for paleo-geological problems.

2. ENVIRONMENTAL BACKGROUND

Our study area lies within the Cretaceous Proto-North Atlantic (Fig.1) which at the time was separated from contemporary ocean basins by sills and narrow seaways. Because of these restricted connections the Proto-North Atlantic probably had a limited deep-water renewal rate and was prone to anoxia (Trabucho Alexandre et al., 2010; Monteiro et al., 2012). Climate modeling, micropaleontological data and geochemical evidence suggest the existence of a productive coastal upwelling system, similar to a modern day OMZ at the northwest African margin in the south-eastern Proto-North Atlantic (e.g. Trabucho Alexandre et al., 2010; Kuhnt et al., 1997; Holbourn et al., 2001; Scholz et al., 2019a). The Tarfaya Basin is located in southern Morocco and provides a record of this upwelling system. It contains a 700 m thick sedimentary succession of Upper Cretaceous organic carbon-rich and partly laminated marls, shales and carbonates. Kolonic et al. (2005) suggest that due to its spatial extent and high organic carbon mass accumulation rates, the Tarfaya Basin represented a globally significant carbon sink. As can be seen from Fig. 1, a variety of sedimentary cores were recovered from the proto-North Atlantic and several within the Tarfaya Basin. Based on organic geochemical evidence in core S57 (Fig.

1), Kolonic et al., (2005) proposed euxinic conditions in the Tarfaya basin during OAE2. Sedimentary Fe speciation data for core S57 also indicate sustained periods of euxinic conditions during OAE2 intersected with ferruginous conditions (Poulton et al., 2015; see also discussion in Section 4).

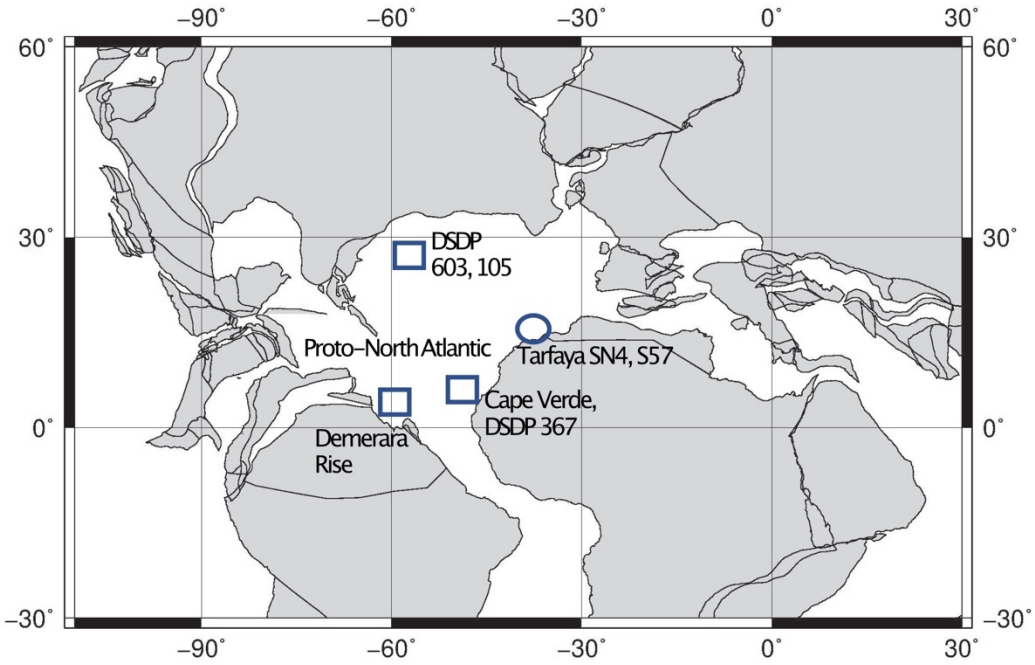

Fig. 1. Study location in the proto-North Atlantic approximately 94Ma ago (ODSN plate tectonic reconstruction service, www.odsn.de). The circle indicates the location of drill core SN4 and S57, squares indicate core locations in publications discussed in the text.

For this study we investigated drill core SN4, located approximately 40 km east of the town of Tarfaya (Kuhnt et al., 2017) and ca 15km further offshore and in slightly deeper water depth than core S57. The paleo-setting of this site during the Cenomanian-Turonian was on the outer shelf at 200 to 300 m water depth. 350 m of sedimentary rocks were recovered corresponding to ca. 5 million years of sedimentation (latest Albian to early Turonian; Beil et al., 2018). OAE2 is represented and marked by a positive organic carbon isotope ($\delta^{13}C_{org}$) excursion (CIE) at a depth of 80 to 110 m (Kuhnt et al., 2017). Average sedimentation rates increased from 4.5 cm/kyr to 7.7 cm/kyr at 120 m depth (Kuhnt et al., 2017). Due to its location close to the outer shelf, core SN4 is thought to have the highest sedimentation rates and organic carbon mass accumulation rates of the cores available from the Tarfaya basin. Moreover, since the sedimentary succession in core SN4 includes a ca. 4 million years

record before the onset of OAE2, we can show how our proxy data evolved for a substantial time before the onset of OAE2.

3. METHODS

For details on the analysis of Mo, Mn and aluminum (Al) concentrations please see details in Scholz et al., 2019a. Analysis of Mo isotopes was performed on a Nu instruments multi collector inductively coupled plasma mass spectrometer using a double isotope tracer (^{100}Mo, ^{97}Mo) for correction of instrumental mass bias (Siebert et al., 2001; see also Scholz et al. (2017) for details). Samples were digested in a mixture of HNO_3, $HClO_4$ and HF. Prior to analyses, Mo was purified by passing the digested sample solutions through cation and anion exchange columns (see Scholz et al., 2017 for details). Isotope ratios of Mo are reported as δ^{98}Mo relative to NIST-SRM-3134 (Nägler et al., 2014). Reference standard SDO-1 (Devonian Ohio Shale, USGS) was processed through column chemistry and measured with each sample run. The error bars plotted in figures correspond to our long-term external reproducibility of SDO-1 (δ^{98}Mo = +0.78 ± 0.09‰ (2SD), n=28). The measured value of δ^{98}Mo = +0.78 is in excellent agreement with previously published values (e.g. Goldberg et al., 2013). Samples were analyzed twice in different analytical sessions and the internal and external errors of sample repeats were within the long-term reproducibility of SDO-1 for all presented samples.

4. RESULTS

An overview of the presented Mo isotope data and corresponding elemental concentration data is given in Table 1. Elemental concentration data for all other depths are given in the supplementary material. Ratios of elements to aluminum (Al) are based on the local Al concentrations measured in core SN4.

The data presented in this study can be divided in four sections of core SN4 that correspond to the evolution of the Tarfaya basin through time (see Discussion, Section 4). During the early Cenomanian (305 to 225m core depth) the average sedimentary Mo concentrations (1.72ppm ± 1.23ppm (1SD), n=35) as well as Mo/Al ratios (0.04 ± 0.03, n=35) are close to crustal values (1.5 ppm and 0.01 respectively; Rudnick & Gao, 2004). TOC is low (1.99% ± 0.72%, n=35) resulting in a low Mo/TOC ratio of 1 ± 0.35 (1SD), n=35). The average manganese (Mn) to Al ratio (0.41 ± 0.36 (1SD), n=35) is half of the crustal ratio (0.8; Rudnick and Gao, 2004). Mo isotopes show a light average δ^{98}Mo of 0.03‰ ± 0.26‰ (1SD), n=7). During the middle Cenomanian (223-111m core depth) a clear increase in sedimentary Mo concentrations (18.34ppm ± 14ppm (1SD), n=48), Mo/Al (1.02 ± 1.04 (1SD), n=48), TOC (5.38% ± 1.82%(1SD), n=48) and therefore the Mo/TOC ratio (3.31 ± 2, n=48) is observed. In addition, the overall signal variability increases. In contrast the average Mn/Al ratio stays virtually constant (0.42 ± 0.2 (1SD), n=48). The average sedimentary Mo isotope composition becomes significantly heavier (δ^{98}Mo = 0.52‰ ± 0.19‰ (1SD), n=15). With the onset of OAE2 (110m-80m core depth), sedimentary Mo concentrations first decrease and then strongly increase in the latter part of OAE 2 (17.92ppm ± 13.68ppm (1SD), n= 12) while sedimentary TOC increases (12.21% ± 3.66% (1SD), n=12) as well as the Mo/Al ratio (2.82 ± 1.8 (1SD), n=12). This results in a lowered Mo/TOC ratio of 1.45 ± 0.82 (1SD, n=12). A shift towards lighter average sedimentary Mo isotope compositions is observed throughout OAE2 (δ^{98}Mo = 0.35‰ ± 0.21‰ (1SD), n=7) coinciding with a significant shift of Mn/Al ratios towards crustal values (0.6 ± 0.27 (1SD), n= 12). At the end of OAE 2 (80 to 46m core depth), average sedimentary Mo concentrations increase (38.88ppm ± 21.04ppm (1SD), n=14), the Mo/Al ratios stay relatively constant (2.33 ± 1.12 (1SD), n=14) while TOC decreases (8.67% ± 1.19% (1SD), n=14) resulting in an average Mo/TOC ratio of 4.41 ± 1.82 (1SD, n=14). The average Mn/Al ratio (0.43 ± 0.12 (1SD), n=14) as well as the Mo isotope composition (δ^{98}Mo = 0.5‰ ± 0.27‰ (1SD), n=6) return to pre-OAE2 values.

5. DISCUSSION

5.1. Molybdenum Cycling in the Tarfaya Upwelling System

5.1.1 Previous Mo isotope studies in the Tarfaya basin, core S57

A number of studies have published geochemical datasets on the Tarfaya basin during OAE2 in particular on core S57 (e.g. Poulton et al., 2015; Goldberg et al., 2016; Dickson et al., 2016). Goldberg et al. (2016) studied in detail a section of core S57 within OAE2 which covers the initial rise in $\delta^{13}C_{org}$ (positive CIE) in the early OAE2 as well as some of the lowest Mo/TOC ratios observed in the area and worldwide at the time (average of approx. 0.7; Goldberg et al., 2016; Kolonic et al., 2005). Goldberg et al. (2016) interpreted their Mo, Mo/TOC and Mo isotope data as being deposited under sustained periods of euxinic conditions interspaced with regular ferruginous episodes, based on Fe speciations (Poulton et al., 2015). In this context, low Mo/TOC ratios that are present despite overall euxinic bottom water conditions which allow highly effective Mo scavenging, are interpreted as an indication for a depleted Mo reservoir (Mo drawdown) either in the proto-North Atlantic or globally. Mo isotope variations presented in Goldberg et al. (2016) span a range from δ^{98}Mo of -0.3 to 1.1‰. However, Mo isotope compositions and euxinic or ferruginous intervals are not correlated. δ^{98}Mo values are relatively constant at 0.6‰ for most of the investigated section. However, interspersed is an episode of light Mo isotope ratios (δ^{98}Mo -0.3 to 0.3‰) followed by an increase to the highest Mo isotope values within the section (up to 1.1‰). Goldberg et al. (2016) interpret heavy Mo isotope values >0.5‰ as the result of near quantitative scavenging of Mo under euxinic conditions with the highest values (i.e. 1.1‰ during OAE2) indicating the minimum seawater Mo isotope composition in the late Cenomanian, which would therefore have been offset to lighter values if compared to the modern ocean (δ^{98}Mo = 2.09‰). Relatively short-term changes of δ^{98}Mo from 0.6‰ to 1.1‰ are, in combination with a low Mo inventory, suggested to indicate a heterogenous distribution of Mo in the late Cretaceous oceans. The section of S57 with comparatively light Mo isotope data (average of δ^{98}Mo at 0.1‰) is difficult to explain within the framework of euxinic to ferruginous conditions. However, Scholz et al. (2019) offers a different interpretation of Fe speciation data in the Tarfaya basin core SN4 during OAE2 that does not require euxinic or ferruginous depositional conditions (see discussion

248 below). In addition, more recent findings suggest that this particular section coincides with a reversal
249 in the CIE, which marks the so called Plenus Cold Event (PCE; e.g. Jenkyns et al., 2017), a time of cooler
250 sea surface temperatures and changing hydrographic conditions in the proto-North Atlantic. Multiple
251 lines of biological and geochemical evidence suggest that the Tarfaya Basin was substantially less
252 reducing during that time or even re-oxygenated (e.g. Kuhnt et al., 2005; Dickson et al., 2016; Jenkyns
253 et al., 2017; Beil et al., 2018; Scholz et al., 2019a). We would therefore suggest that the light Mo isotope
254 signature during that time is caused by more oxidizing depositional conditions where Mo is scavenged
255 in association with Mn and/or Fe oxy-(hydroxides).

256 The focus of a study by Dickson et al. (2016) was on Site 367 in the deep Cape Verde basin. However,
257 they also present data from core S57. At Site 367, among other proxies, the observed high sedimentary
258 Mo/U ratios (2 to 10 times higher than present day seawater) suggests euxinic bottom waters during
259 OAE2 (Algeo and Tribovillard, 2009). Mo isotopes compositions in the Cape Verde basin center around
260 δ^{98}Mo of 0‰ before the onset of OAE2 and rise up to δ^{98}Mo of 1.2‰ after the onset of OAE2. This
261 value is also interpreted by Dickson et al. (2016) as the δ^{98}Mo signature of global seawater during
262 OAE2. Mo isotope compositions during the main plateau of OAE2 show a pattern oscillating between
263 δ^{98}Mo of 0.5‰ and 1.1‰, where low Mo/TOC and low Mo/U ratios are correlated with the low δ^{98}Mo
264 signals. The authors interpret this feature as the result of periodic changes in the (local) Proto-North
265 Atlantic Ocean dissolved Mo inventory and/or the basins dissolved H_2S concentration. The observed
266 cycling of δ^{98}Mo values would then be caused by either variation in the rate of seawater exchange with
267 the global ocean or changes in local productivity due to altered nutrient supply to the proto-North
268 Atlantic region. The authors estimate that in order to explain the relatively fast changes in δ^{98}Mo in
269 the Cape Verde basin, the global ocean Mo inventory would have to be at 5 to 10% of the modern
270 seawater Mo inventory.

271 For the Tarfaya core S57, the authors do not see major variations in δ^{98}Mo and values tend to center
272 around 0.5‰, which is similar to the lower value of δ^{98}Mo variations observed in the Cape Verde basin
273 and at other sites around the proto-North Atlantic (Westermann et al., 2014). Dickson et al. (2016)

suggest that this value is more indicative of Mo deposition in sulphidic sediments rather than sulphidic bottom water conditions (euxinia). Therefore, if a fractionation of $\Delta^{98}Mo_{sediment\text{-}seawater}$ of 0.8‰ is applied, the resulting seawater Mo isotope composition would be $\delta^{98}Mo$ = 1.3‰ (e.g. Siebert et al., 2006, Poulson-Brucker et al., 2009). This would also imply that the Tarfaya basin was less hydrographically restricted than the Cape Verde basin.

5.1.2 This study, core SN4

Our study presents Mo/TOC as well as manganese (Mn) concentration data and Mo isotope data for core SN4 in the Tarfaya basin for a 5Ma time span ranging from the beginning of the Cenomanian to the end of OAE2 in the Turonian. The Tarfaya basin has been considered a paleo-upwelling setting in previous studies (e.g. Kolodnic et al., 2005; Westermann et al., 2014; Kuhnt et al., 1997; Holbourn et al., 2001; Scholz et al., 2019a). Although Poulton et al., 2015 and Goldberg et al., 2016 interpreted Site S57 as deposited under euxinic to ferruginous conditions, we argue that core SN4 was deposited under nitrogenous conditions in a dynamic upwelling system similar to modern day OMZ's like the Peruvian margin or the Namibian Shelf. This line of reasoning is based on the following considerations. Combining nitrogen isotope data and Fe speciation data on core SN4, Scholz et al. (2019a) showed that the observed elevated Fe_{HR}/Fe_T and Fe_T/Al ratios are more likely explained by transport-limited chemical weathering in the Cretaceous greenhouse climate, than Fe precipitation from anoxic seawater. Transport-limited weathering under these conditions would result in a low but highly weathered flux of terrigenous material enriched in Fe (oxyhydr)oxide minerals. Therefore, a relatively low authigenic Fe rain rate and a moderate sulfate reduction rate could produce a Fe_{HR}/Fe_T and Fe_P/Fe_{HR} signature which would commonly be interpreted as ferruginous, but is in this context consistent with nitrogenous (i.e. denitrifying) conditions (Scholz et al., 2014; 2019a).

Directly applied to the redox evolution of the Tarfaya basin as sampled by core SN4, the early to middle Cenomanian is characterized by low concentrations of organic carbon and redox-sensitive metals as

well as low Fepy/FeHR, indicating oxic bottom water conditions at the time of deposition (Scholz et al., 2019a).

During the middle Cenomanian and thereafter (above ~225 m downcore depth) generally increasing Fe_{HR}/Fe_T, Fe_P/Fe_{HR} (Scholz et al., 2019a) and increasing enrichment of TOC and Mo over crustal background as well as higher Mo/TOC ratios (this study; Fig. 3) indicate oxygen-deficient conditions in the bottom water, suggesting that the transition towards an oxygen-depleted upwelling system started in the mid-Cenomanian (see also Beil et al., 2018). Based on Fe speciation data, conditions remained nitrogenous or weakly sulfidic throughout the OAE2 section of core SN4, while the Mo/TOC ratios substantially decrease after the onset of OAE2. We therefore postulate, that Mo proxy signals in our core have to be interpreted in the context of denitrifying to mildly sulfidic conditions in an OMZ before and during OAE2.

A second line of reasoning derives from the range of sedimentary enrichment factors of TOC and Mo concentrations also expressed as Mo/TOC ratios observed in core SN4.

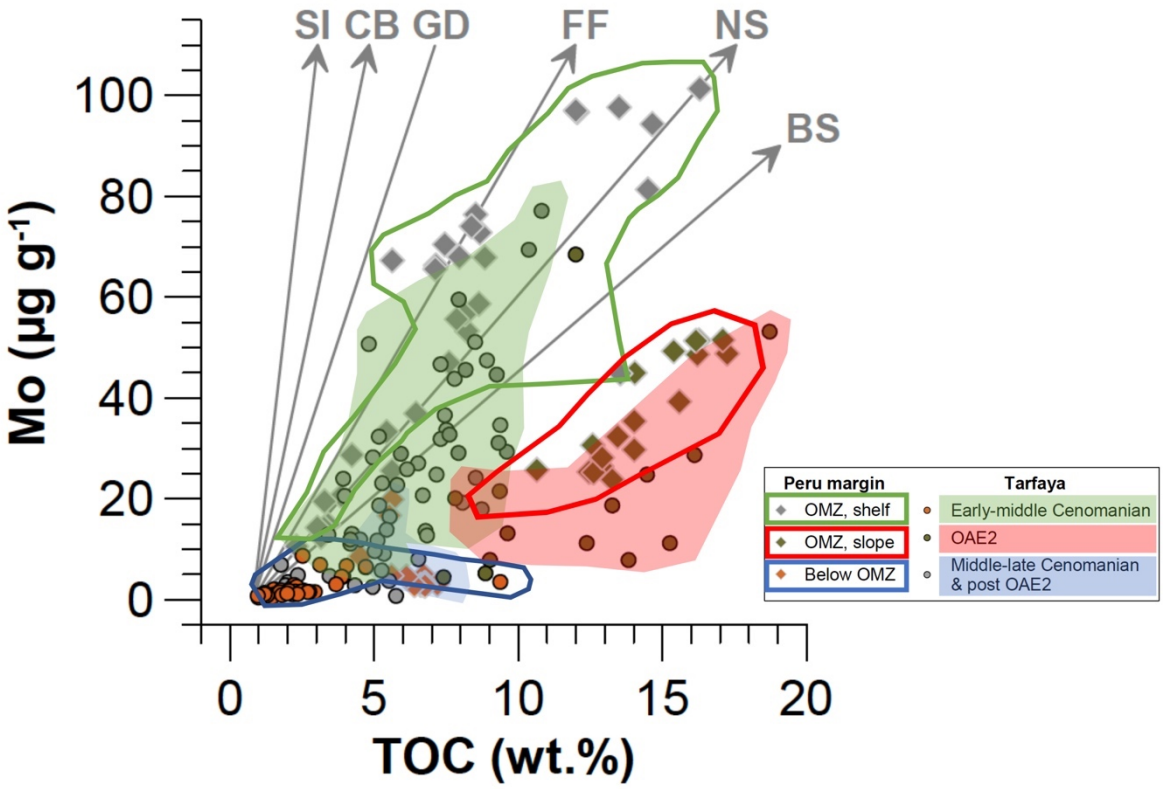

Fig. 2. Plot of sedimentary Mo concentrations versus Mo/TOC showing data for shallow sediment cores from the Peruvian margin (Scholz et al., 2017) and core SN4 from the Tarfaya upwelling system in the late Cretaceous Proto-North Atlantic. Gray arrows represent the Mo/TOC co-variation trends observed in other anoxic marine systems (SI: Saanich Inlet, GB: Cariaco Basin, GD: Gotland Deep, Baltic Sea, FF: Framvaren Fjord, NS: Namibian Shelf, BS: Black Sea) (Algeo and Lyons, 2006; Scholz et al., 2018).

Having established above that we interpret the Tarfaya basin as an upwelling system, we would like to explicitly state that we are not using Mo/TOC ratios as a measure of basin restriction as originally suggested by Algeo and Lyons 2006 (see also Section 1). Instead we point out that modern day upwelling areas like the Peruvian upwelling zone also display systematic variations in the Mo/TOC ratio.

In Fig. 2 we show Mo and TOC data from the modern OMZ in Peru. Within this upwelling system a variety of Mo/TOC ratios are present in geographical proximity at the same time, depending on the relative position of the sampled core with respect to the OMZ (Scholz et al., 2017). Mo/TOC ratios from

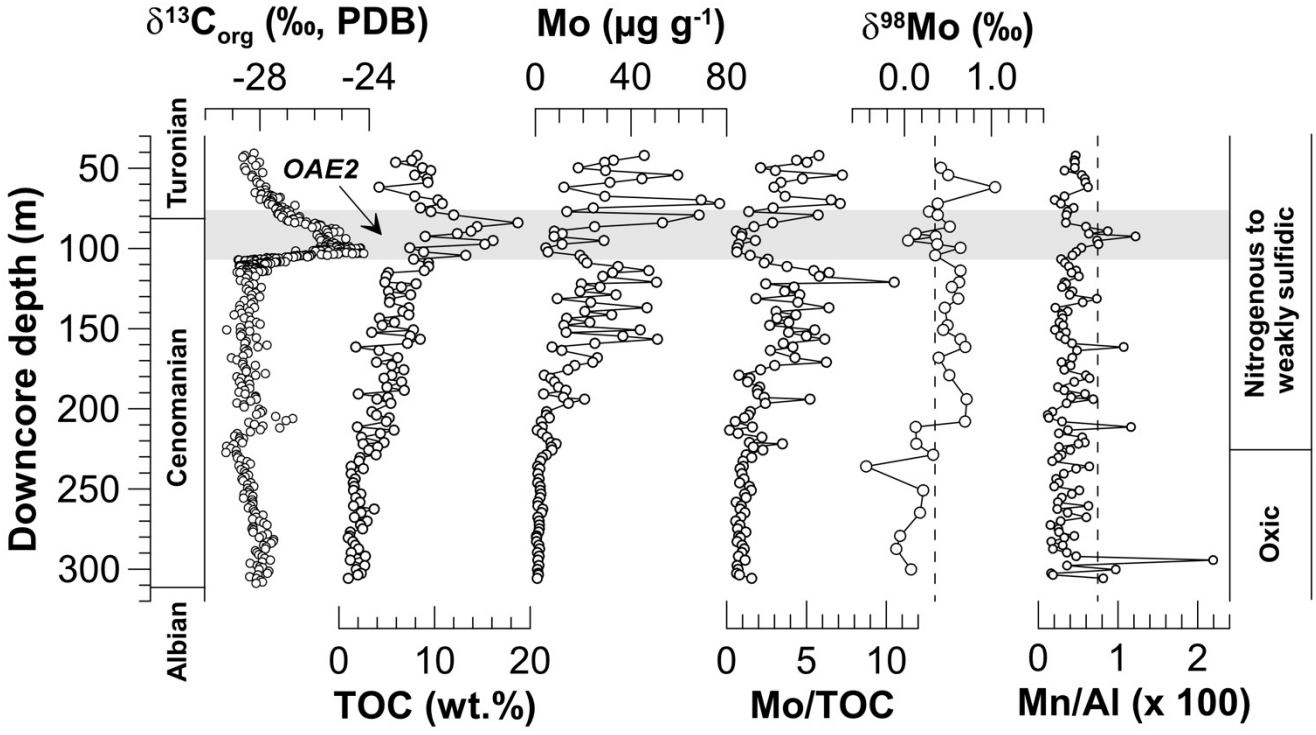

Fig. 3. Proxy records for core SN4 from the Tarfaya upwelling system in the late Cretaceous Proto-North Atlantic: Isotope composition of organic carbon ($\delta^{13}C_{org}$) (Beil et al., 2018), TOC (Scholz et al., 2019a), Mo, Mo/TOC, δ^{98}Mo and Mn/Al. Vertical dashed lines represent the δ^{98}Mo (Voegelin et al., 2014) and Mn/Al (McLennan, 2001; Rudnick & Gao, 2004) of upper continental crust.

below the OMZ represent oxygenated bottom water and closely resemble the Mo/TOC range observed in SN4 before the onset of reducing conditions in the middle Cenomanian (below 220m sample depth). During the middle to late Cenomanian (~220 - 120 m) and after OAE2, Mo/TOC ratios from SN4, in line with the evidence from Fe speciation proxies, resemble those observed on the Peru shelf within the main OMZ where conditions are nitrogenous to weakly sulfidic. Overall, these parallels suggest that the Mo cycle in Tarfaya operated similarly to that in modern coastal upwelling systems during that time.

Between ~120 m and the onset of OAE2, a steep drop in Mo/TOC is observed (Fig. 3). Goldberg et al. (2016) attributed the low Mo/TOC during OAE2 to Mo depletion in the water column. Very low Mo/TOC ratios observed at other locations in the proto-North Atlantic (Mo/TOC of 1 to 5; Kuypers et al., 2004; Hetzel et al., 2009; Westermann et al., 2014) and sulfur isotopes indicating massive pyrite burial during OAE2 (e.g. Owens et al, 2013) support this scenario. However, this interpretation cannot easily account for the differences in proxy signals (Mo/TOC, Mo isotope compositions, see below) between cores SN4 and S57 in the Tarfaya basin over short geographical distances. By considering the Tarfaya basin as a dynamic upwelling area rather than a classic restricted basin we suggest that that the shift in Mo/TOC ratios in core SN4 at the onset of OAE2 could be explained by a shift of the relative OMZ position and/or its boundaries. Consistent with this scenario, sedimentary Mo concentrations and Mo/TOC observed in Tarfaya around the onset of OAE2 are similar to those found on the Peruvian upper slope and at the lower boundary of the Peruvian OMZ indicating low oxygen conditions (Fig. 2). Increasing Mo/TOC ratios and Mo isotope ratios towards the end of OAE2 could then indicate a reversal to pre-OAE2 conditions at the end of OAE2 (Fig. 3).

The scenario described above for the redox evolution of the Tarfaya basin during the late Cretaceous is strongly supported by our Mo isotope data. During the early Cenomanian δ^{98}Mo values average 0‰. Light Mo isotope compositions, in particular lighter than the riverine input (δ^{98}Mo = 0.4‰) are associated with Mo isotope fractionation via Mn and/or Fe oxy-(hydroxides) indicating oxygenated bottom water conditions during time of deposition (e.g. Siebert et al., 2003; Barling et al., 2004; Wasylenki et al., 2011). The offset to somewhat heavier Mo isotope composition when compared to modern day Fe-Mn crusts (δ^{98}Mo of ~-0.8‰) is probably due to mixing of the authigenic Mo signal with a detrital signal at low sedimentary Mo concentrations.

With the start of the nitrogenous depositional conditions in the middle Cenomanian as indicated by Mo/TOC, Fe speciation and nitrogen isotope data (this study; Scholz et al., 2019a), the average Mo isotope composition of the deposited sediments shifts to a δ^{98}Mo of 0.5‰. This isotope shift is consistent with the transition to anoxic conditions. This Mo isotope signal then remains relatively constant until the onset of OAE2. Many modern anoxic sediments cluster around a δ^{98}Mo of 1.4‰ and are therefore offset from seawater by +0.8‰ (expressed as $\Delta^{98}Mo_{sediment\text{-}seawater}$ = +0.8‰). Applied to the middle Cenomanian sedimentary signal of δ^{98}Mo = +0.5‰, this would result in a seawater isotope signature of approximately 1.3‰. However, the observed average anoxic sedimentary Mo isotope signal at the Peruvian continental margin is δ^{98}Mo = +1.03 ± 0.10‰ ((1 SD), n = 21; Scholz et al., 2017). Applying this offset (+1.06‰) to the Tarfaya data results in a late Cretaceous Mo isotope seawater signature of approximately +1.6‰.

Our data therefore show a substantially lighter global seawater Mo isotope composition with respect to modern day values millions of years before the onset of OAE2, indicating changes in the global seawater Mo isotope mass balance. Very recently Dickson et al., 2021 reported a similar data set for Mo isotope compositions from the northern proto-North Atlantic (Eagle Ford Group, Southern Texas) spanning a similar time range than Site SN4. Their data show relatively constant Mo isotope values centering around a δ^{98}Mo of 0.5‰ pre-OAE2. Their estimated seawater isotope ratio based on a comparison of their paleo-environmental setting with the modern day Cariaco Basin is 1.1 to 1.9‰

(δ^{98}Mo), similar to our estimate of 1.6‰ (δ^{98}Mo). We will attempt to explain this light pre-OAE2 Mo seawater isotope ratio in Section 5.2.

The pre-OAE2 Mo isotope data presented above and by Dickson et al., 2021 are close to Mo isotope seawater compositions postulated by Dickson et al., 2016 and Goldberg et al., 2016 during the OAE2 itself (1.4‰ to 1.1‰). In addition, the sedimentary Mo isotope signal directly observed at Site S57 during large parts of OAE2 (with exception of the PCE) by both Dickson et al. (2016) and Goldberg et al. (2016) averages around values of 0.5‰ to 0.6‰, respectively, similar to the signal observed in the middle Cenomanian in this study (see above) and by Dickson et al. (2016) for the sulfide fractionated Mo isotope values at Site 367. The consistency of this anoxic δ^{98}Mo signal in core S57, core SN4 pre-OAE2 and the Cape Verde basin indicates that the δ^{98}Mo of seawater during OAE2 might not have shifted considerably from pre-OAE values, a conclusion also reached by Dickson et al., 2021. Dickson et al. (2021) explain the discrepancy between observations of global expansion in euxinic sedimentation at the onset of OAE2 and the relatively small change in Mo seawater isotope compositions (maximum 0.4‰; Dickson et al., 2021) by a balancing increase of burial of light Mo associated with Fe-oxyhydroxides in low-oxygen water masses with increased supply of Fe from increased continental weathering. This interpretation is based on seawater OAE2 Mo isotope estimations from the Cape Verde basin (Dickson et al., 2016).

We observe a decrease in δ^{98}Mo after the onset of OAE2 at Site SN4 with Mo isotope compositions intermittently approaching δ^{98}Mo of 0‰ and averaging at +0.3‰. In contrast, Mo isotopes at Site S57 (Goldberg et al., 2016; Dickson et al., 2016) are similar to those observed pre-OAE2 in core SN4 (see also above).

In the specific case of our core SN4 we do not observe a change in Fe speciation during OAE2 (Scholz et al., 2019a), therefore we do not see direct evidence of increased Fe delivery into the Tarfaya Basin during OAE2. In addition, Site SN4 and S57 are geographically only 15km apart at somewhat different water depth, but show a difference of, on average, 0.2‰ in Mo isotope compositions during OAE2, which cannot easily be explained by overall changes in the seawater Mo isotope mass balance.

Therefore, we would like to put forward a scenario that is more consistent with our observations. The light Mo isotope compositions during OAE 2 coincide with a broad peak in Mn/Al at Site SN4 (Fig. 3). Due to reductive Mn dissolution and offshore transport, sediments in modern OMZs are typically depleted in Mn relative to terrigenous material (i.e., Mn/Al < continental crust) (Brumsack, 2006). By contrast, below the OMZ reductive Mn loss is less efficient so that sedimentary Mn/Al can resume crustal values (Scholz et al., 2019b). Molybdenum adsorbed to Mn oxides has a light isotope composition (Siebert et al., 2003; Barling et al., 2004; Wasylenki et al., 2011). Successive shifts in Mo/TOC (Fig. 1), δ^{98}Mo and Mn/Al after the onset of OAE2 are, thus, consistent with a shallowing of the OMZ, possibly connected to changes in sea level and/or atmospheric and ocean circulation (e.g., Deutsch et al., 2014). It is important to note that such a scenario could account for the difference in Mo isotope compositions of Sites S57 and SN4 during the same time interval as well as the very low Mo/TOC ratios observed by Goldberg et al. (2016) and Kolonic et al (2005).

We are aware that our profile shows several Mn concentration spikes before the onset of OAE2, However, these spikes are due to one single measurement and do not show a wider trend like the Mn excursion during OAE2. In addition, Mo isotope values that were measured from some of the same sample aliquots as the high Mn concentrations before OAE2 do not show any light “anomalies”. A possible exception is the sample from 236m sample depth. This negative Mo isotope excursion and the associated small Mn peak might indicate a higher rate of bottom water oxygenation at that time.

In summary we can state, that a stable upwelling system analogous to a modern OMZ was in place in the Tarfaya basin in the late Cretaceous before the onset of OAE2 (e.g. Kuhnt et al., 1997; Beil et al., 2018; Scholz etal., 2019a) and that at that time the Mo isotope composition of the global ocean was already lower than today. Because there are indications for expanding global anoxia (e.g. Demerara Rise, Hetzl et al., 2009) but no indications for massive global drawdown of Mo from seawater or lowering of the Mo/TOC ratio before OAE2 (e.g. Owens et al., 2016), we suggest an alternative scenario for the evolution of late Cretaceous seawater and the associated changes in global oceanic redox conditions based on the reduction of Mn burial in oxic sediments.

433

434 **4.2. Molybdenum Inventory of the late Cretaceous Ocean**

435 Our analysis of Mo cycling in the Tarfaya upwelling system suggests that late Cretaceous pre- OAE2
436 seawater had a lighter δ^{98}Mo (~+1.3‰ to ~+1.6 ‰) than modern seawater ($\Delta^{98}Mo_{sediment\text{-}seawater}$ of
437 0.8‰ to 1.06‰). Based on the similarities of the Tarfaya OMZ with the modern day Peruvian
438 continental margin, we consider a δ^{98}Mo of 1.6‰ in seawater a more realistic option for the middle
439 Cenomanian and post OAE2 ocean.

440 Following a classic mass balance approach, δ^{98}Mo in seawater at steady state is a function of the Mo
441 input flux via rivers (F_{in}), its isotope composition ($\delta^{98}Mo_{river}$), Mo burial fluxes into oxic (F_{ox}) and anoxic
442 (F_{anox}) marine sediments and the associated isotope fractionation factors ($\Delta^{98}Mo_{seawater\text{-}sediment}$):

443 $$\delta^{98}Mo_{seawater} = \delta^{98}Mo_{river} + \frac{F_{ox}}{F_{in}} \cdot \Delta^{98}Mo_{seawater-sediment} + \frac{F_{anox}}{F_{in}} \cdot \Delta^{98}Mo_{seawater-sediment} \quad (1)$$

444 Adopting the modern F_{in} ($3.09 \cdot 10^8$ mol yr^{-1}) (Miller et al., 2011) and $\delta^{98}Mo_{river}$ (+0.4 ‰) (Archer and
445 Vance, 2008) as well as $\Delta^{98}Mo_{seawater\text{-}sediment}$ of +3 ‰ for oxic sediments (Barling et al, 2001, Siebert et
446 al., 2003; Barling et al., 2004; Goldberg et al., 2016) and +0.8 ‰ for anoxic sediments (Poulson-Brucker
447 et al., 2009; Scholz et al., 2017) yields F_{ox} = $1.33 \cdot 10^8$ mol yr^{-1} and F_{anox} = $1.76 \cdot 10^8$ mol yr^{-1} and a
448 seawater Mo isotope composition of 2.08‰. This combination of burial fluxes, corresponding to 43 %
449 oxic and 57 % anoxic Mo burial, is broadly consistent with earlier studies (e.g., Goldberg et al., 2016
450 and references therein). We are aware that the Mo inventory during the late Cretaceous was not
451 necessarily the same as today, however because the Cretaceous Mo seawater budget cannot be
452 constrained we applied a modern "starting point" for our model similar to previous studies (e.g.
453 Goldberg et al., 2016; Dickson et al., 2016). We do not explicitly consider a euxinic Mo sink, because
454 the $\Delta^{98}Mo_{seawater\text{-}sediment}$ observed in these environments is mostly similar to those in anoxic systems
455 without hydrogen sulfide in the water column (Arnold et al., 2004; Neubert et al., 2008; Noordmann
456 et al., 2015; Scholz et al., 2018).

Following the approach of previous paleo-studies, including studies in the proto-North Atlantic, it is possible to calculate a lower Cretaceous δ^{98}Mo of 1.6‰ for seawater by increasing the flux of Mo into anoxic marine sediments only. A δ^{98}Mo of 1.6‰ is attained by increasing the anoxic Mo flux (F_{anox}) 2.7 times (Fig. 4a). The average concentration of Mo in seawater ($[Mo]_{seawater}$) corresponding to this scenario can be calculated from the modern seawater Mo concentration ($[Mo]_{modern}$) and the modern and modified burial fluxes:

$$[Mo]_{seawater} = [Mo]_{modern} \cdot \frac{(F_{ox}+F_{anox})_{modern}}{(F_{ox}+F_{anox})_{modified}} \quad (2)$$

Increasing F_{anox} by a factor of 2.7 and keeping F_{ox} constant results in a global seawater Mo inventory of ca. 50% (52nM) of the modern day. Given the fact that there is no indication of massive Mo drawdown and changes in the seawater Mo inventory in the middle Cenomanian (e.g. Owens et al., 2016), we consider this scenario by itself as highly unlikely.

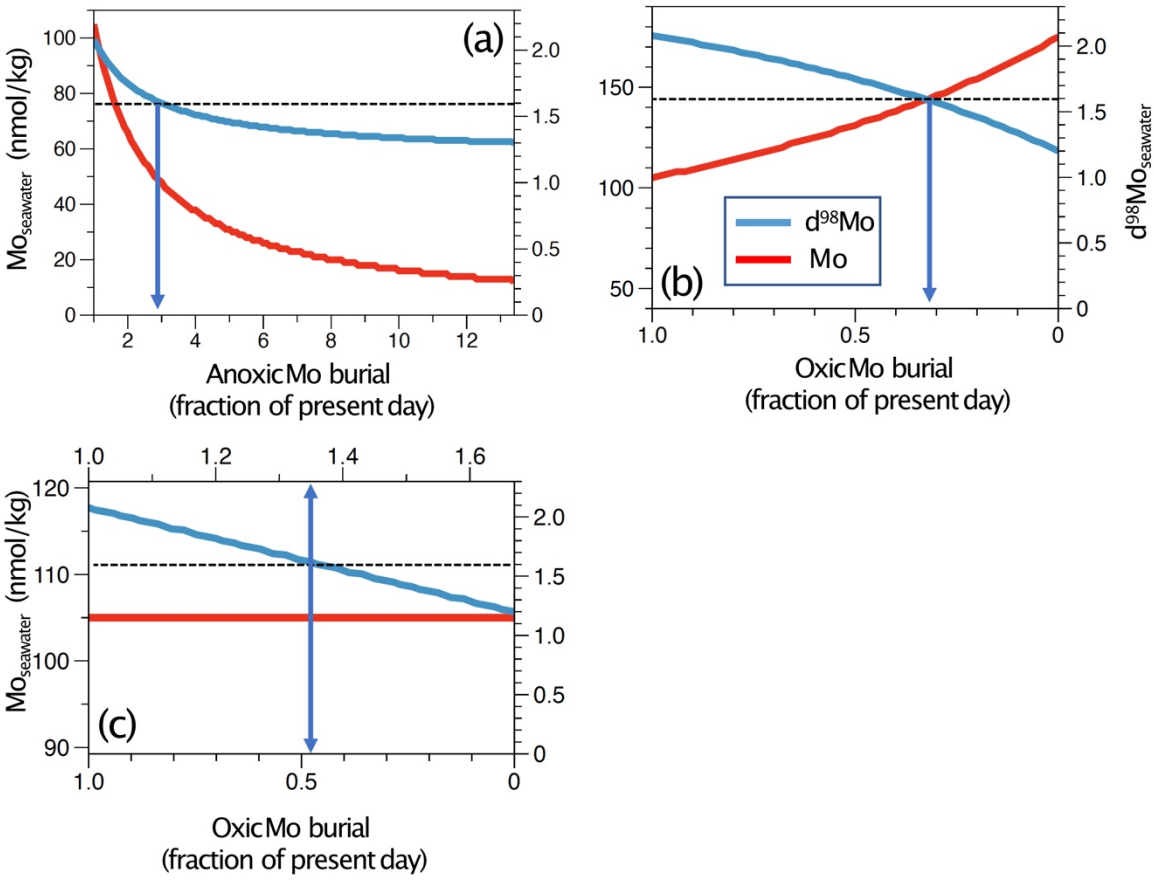

Fig. 4. Modelled seawater Mo concentrations and isotope compositions in the late Cretaceous as a function of the fraction of Mo burial under oxic and anoxic conditions relative to the present-day (a,b,c). Horizontal dashed lines represent inferred Mo isotope compositions of the late Cretaceous ocean (this study, $\delta^{98}Mo_{seawater}$ of +1.6‰). (a) Scenario with increased anoxic Mo burial. (b) Scenario with decreased oxic Mo burial. (c) Scenario with both increased anoxic and decreased oxic Mo burial (top x-axis label the same as lower x-axis label in (a)), Mo concentration as present day.

We propose that oxic Mo burial associated with Mn oxides in the usually well oxygenated deep-sea would be reduced under conditions of globally expanded anoxia. There is clear evidence for reduced Mn burial in the poorly oxygenated Southern Ocean during the last ice age (Jaccard et al., 2016). In addition, sedimentary thallium isotope systematics indicate reduced Mn oxide burial during OAE2 (Ostrander et al., 2017). Thallium isotopes fractionate during adsorption to Mn oxy-(hydroxides) and the resulting isotope signals are not easily altered by subsequent secondary processes. Therefore, perturbations of the Mn oxide precipitation cycle are archived in sediments deposited under oxic conditions. Ostrander et al., (2017) see a clear shift in Tl isotope values shortly before the onset of OAE2 and model a reduction of Mn oxide precipitation by 40 to 80%. However, the authors also observe that the Tl isotope composition of sediments before this shift at the onset of OAE2 is already significantly offset from modern day values. Therefore, it seems likely that a substantial reduction of Mn oxide precipitation in the open ocean already occurred during the late Cretaceous. As an admittedly extreme scenario, a δ^{98}Mo of +1.6‰ in seawater could be generated with the modern F_{anoxic} but a 70 % reduction of F_{ox} (Fig. 4b). This scenario would result in an increased rather than decreased seawater Mo concentration.

We consider both of the above scenarios as unlikely to be representative for a natural deoxygenation event. Instead, we suggest that anoxic Mo burial increased at the expense of oxic Mo burial. While $\delta^{98}Mo_{seawater}$ would be lowered in such a scenario, Mo concentrations would remain virtually constant. For example, a modern seawater Mo concentration and a δ^{98}Mo of +1.6‰ can be attained by decreasing F_{ox} by ~55 % and increasing F_{anox} by ~35 % (Fig. 4c). We also point out that a reduction of the oxic Mn sink in the deep ocean would have resulted in a larger Mn inventory in the ocean and, by inference, increased upwelling of Mn at continental margins, which could have delivered additional

Mn contributing to the broad Mn peak and negative Mo isotope excursion (Fig. 3) observed in Tarfaya during OAE2.

This scenario can explain the observed change in the Mo isotope mass-balance prior to OAE2 (Dickson et al., (2021); this study) A further decrease of Mn burial rates in the open ocean during the OAE2 event as indicated by Tl isotope considerations (Ostrander et al., 2017, see also above) could then have "buffered" the Mo seawater isotope signal during OAE2, explaining the relatively small difference in seawater Mo isotope compositions between pre-OAE2 and OAE2 values observed in the proto North Atlantic.

6. CONCLUSIONS

Based on the similarity of covariation pattern of Mo and TOC in sediments of the Tarfaya basin and the modern Peruvian continental margin, we can conclude that the Mo cycle in the Tarfaya upwelling system operated similar to that in modern anoxic upwelling systems. Consistent with prior studies, we demonstrate that depositional conditions in the Tarfaya basin became anoxic and an OMZ was established in the middle Cenomanian millions of years before the onset of OAE2. Our data indicate that during this time the Mo isotope composition of global seawater was lighter compared to the present-day ($\Delta^{98}Mo_{modernSW\text{-}CretaceousSW}$ = +0.5‰). Because pre-OAE sediments show enrichment in Mo, but no indication of a massive Mo drawdown we explain global lowering of the Mo isotope composition of seawater with small or no changes in the ocean Mo inventory by a reduced Mn burial rate and therefore decreased Mo burial into oxic deep-sea sediments and moderately increased Mo burial into anoxic sediments. A further decrease of Mn burial rates in the open ocean during OAE2 could then buffer the Mo seawater isotope signal during OAE2, explaining the relatively small difference in seawater Mo isotope compositions between pre-OAE2 and OAE2 values observed in the proto North Atlantic.

This scenario emphasizes that changes to the relative size of not only the anoxic sink but also the oxic sink are important considerations when interpreting paleo-Mo isotope data.

ACKNOWLEDGEMENTS

The first author would like to thank Jan Kramers for a fantastic start into the world of isotopes and for conveying the enthusiasm to explain global environmental change with tiny variations in the isotopes of trace elements (which have names that are difficult to pronounce). In Jan Kramers spirit this study is intended to inspire readers to sometimes look at a geological problem from a different point of view.

Jeremy Owens and an anonymous reviewer are thanked for constructive reviews that greatly improved this publication. We would also like to thank Anna-Kathrin Retschko and Regina Surberg for laboratory assistance. This work was supported by the German Research Foundation (DFG) through Emmy Noether Research Group ICONOX (Iron Cycling in Continental Margin Sediments and the Nutrient and Oxygen Balance of the Ocean) and Collaborative Research Centre 754 (Climate-Biogeochemistry Interactions in the Tropical Ocean).

REFERENCES

Algeo, T.J., Lyons, T.W., 2006. Mo-total organic carbon covariation in modern anoxic marine environments: Implications for analysis of paleoredox and paleohydrographic conditions. Paleoceanography, 21(1).

Algeo, T.J., Tribovillard, N., 2009. Environmental analysis of paleoceanographic systems based on molybdenum-uranium covariation. Chemical Geology, 268(3-4): 211-225.

Archer, C., Vance, D., 2008. The isotopic signature of the global riverine molybdenum flux and anoxia in the ancient oceans. Nature Geoscience, 1(9): 597-600.

Arnold, G.L., Anbar, A.D., Barling, J., Lyons, T.W., 2004. Molybdenum isotope evidence for widespread anoxia in mid-proterozoic oceans. Science, 304(5667): 87-90.

Arthur, M.A., Schlanger, S.O., 1985. Variations in the global carbon cycle during the Cretaceous related to climate, volcanism and changes in atmospheric CO2, The Carbon Cycle and Atmospheric CO2: Natural Variations, Archean to Present, pp. 504-529.

Barling, J., Anbar, A.D., 2004. Molybdenum isotope fractionation during adsorption by manganese oxides. Earth and Planetary Science Letters, 217(3-4): 315-329.

Barling, J., Arnold, G.L., Anbar, A.D., 2001. Natural mass-dependent variations in the isotopic composition of molybdenum. Earth and Planetary Science Letters, 193(3-4): 447-457.

554 Beil, S. et al., 2018. New insights into Cenomanian paleoceanography and climate evolution from the Tarfaya
555 Basin, southern Morocco. Cretaceous Research, 84: 451-473.
556 Brumsack, H.J., 2006. The trace metal content of recent organic carbon-rich sediments: Implications for
557 Cretaceous black shale formation. Palaeogeography Palaeoclimatology Palaeoecology, 232(2-4): 344-
558 361.
559 Brüske, A., Weyer, S., Zhao, M.Y., Planavski, N.J., Wegwerth, A., Neubert, N., Dellwig, O., Lau, K.V.,
560 Lyons, T.W., 2020. Correlated molybdenum and uranium isotope signatures in moder anoxic
561 sediments: Implications for their use as paleo-redox proxy. Geochimica Et Cosmochimica Acta, 270:
562 449.474.
563 Crusius, J., Calvert, S., Pedersen, T., Sage, D., 1996. Rhenium and molybdenum enrichments in sediments as
564 indicators of oxic, suboxic and sulfidic conditions of deposition. Earth and Planetary Science Letters,
565 145(1-4): 65-78.
566 Dahl, T.W. et al., 2017. Evidence of molybdenum association with particulate organic matter under sulfidic
567 conditions. Geobiology, 15(2): 311-323.
568 Deutsch, C. et al., 2014. Centennial changes in North Pacific anoxia linked to tropical trade winds. Science,
569 345(6197): 665-668.
570 Dickson, A.J., 2017. A molybdenum-isotope perspective on Phanerozoic deoxygenation events. Nature
571 Geoscience, 10(10): 721-726.
572 Dickson, A.J. et al., 2016. Basin-scale controls on the molybdenum-isotope composition of seawater during
573 Oceanic Anoxic Event 2 (Late Cretaceous) (vol 178, pg 291, 2016). Geochimica Et Cosmochimica
574 Acta, 189: 404-405.
575 Dickson, A.J., Jenkyns, H.C., Idiz, E., Sweere, T.C., Murphy, M.J., van den Boorn, S., Ruhl, M., Eldrett, J.S.,
576 Porcelli, D., 2021. New Constrains on Global Geochemical Cyling During Ocean Anoxic Event 2
577 (Late Cretaceous) From a 6-Million-Year Long Molybdenum Isotope Record. G3, 22,
578 e2020GC009246et al., 2021
579 Eroglu, S., Scholz, F., Frank, M., Siebert, C., 2020. Influence of particulate versus diffusive molybdenum
580 supply mechanisms on the molybdenum isotope composition of continental margin sediments.
581 Geochimica Et Cosmochimica Acta, 273: 51-69.
582 Friedrich, O., Norris, R.D., Erbacher, J., 2012. Evolution of middle to Late Cretaceous oceans-A 55 m.y.
583 record of Earth's temperature and carbon cycle. Geology, 40(2): 107-110.
584 Goldberg, T. et al., 2012. Controls on Mo isotope fractionations in a Mn-rich anoxic marine sediment, Gullmar
585 Fjord, Sweden. Chemical Geology, 296: 73-82.
586 Goldberg, T. et al., 2013. Resolution of inter-laboratory discrepancies in Mo isotope data: an intercalibration.
587 Journal of Analytical Atomic Spectrometry, 28(5): 724-735.
588 Goldberg, T., Poulton, S.W., Wagner, T., Kolonic, S.F., Rehkamper, M., 2016. Molybdenum drawdown
589 during Cretaceous Oceanic Anoxic Event 2. Earth and Planetary Science Letters, 440: 81-91.

590 Hardisty, D.S., Lyons, T.C., Riedinger, N., Isson, T.T., Owens, J.D., Aller, R.C., Rye, D.M.,
591 Planavsky, N.J., Reinhard, C.T., Gill, B.C., Masterson, A.L., Asael, D., Johnston, D.T. An evaluation
592 of sedimentary molybdenum and iron as proxies for pore fluid paleoredox conditions. American
593 Journal of Science, 318 (5) 527-556

594 Helz, G.R., Bura-Nakic, E., Mikac, N., Ciglenecki, I., 2011. New model for molybdenum behavior in euxinic
595 waters. Chemical Geology, 284(3-4): 323-332.
596 Hetzel, A., Bottcher, M.E., Wortmann, U.G., Brumsack, H.J., 2009. Paleo-redox conditions during OAE 2
597 reflected in Demerara Rise sediment geochemistry (ODP Leg 207). Palaeogeography
598 Palaeoclimatology Palaeoecology, 273(3-4): 302-328.
599 Holbourn, A., Kuhnt, W., Soeding, E., 2001. Atlantic paleobathymetry, paleoproductivity and paleocirculation
600 in the late Albian: the benthic foraminiferal record. Palaeogeography Palaeoclimatology
601 Palaeoecology, 170(3-4): 171-196.
602 Jaccard, S.L., Galbraith, E.D., Martinez-Garcia, A., Anderson, R.F., 2016. Covariation of deep Southern
603 Ocean oxygenation and atmospheric CO2 through the last ice age. Nature, 530(7589): 207-+.
604 Jenkyns, H.C., 2010. Geochemistry of oceanic anoxic events. Geochemistry Geophysics Geosystems, 11.

Jenkyns, H.C., Dickson, A.J., Ruhl, M., Van den Boorn, S., 2017. Basalt-seawater interaction, the Plenus Cold Event, enhanced weathering and geochemical change: deconstructing Oceanic Anoxic Event 2 (Cenomanian-Turonian, Late Cretaceous). Sedimentology, 64(1): 16-43.

Kolonic, S. et al., 2005. Black shale deposition on the northwest African Shelf during the Cenomanian/Turonian oceanic anoxic event: Climate coupling and global organic carbon burial. Paleoceanography, 20(1).

Kuhnt, W. et al., 2017. Unraveling the onset of Cretaceous Oceanic Anoxic Event 2 in an extended sediment archive from the Tarfaya-Laayoune Basin, Morocco. Paleoceanography, 32(8): 923-946.

Kuhnt, W., Nederbragt, A., Leine, L., 1997. Cyclicity of Cenomanian-Turonian organic-carbon-rich sediments in the Tarfaya Atlantic Coastal Basin (Morocco). Cretaceous Research, 18(4): 587-601.

Kuypers, M.M.M. et al., 2004. Orbital forcing of organic carbon burial in the proto-North Atlantic during oceanic anoxic event 2. Earth and Planetary Science Letters, 228(3-4): 465-482.

McLennan, S.M., 2001. Relationships between the trace element composition of sedimentary rocks and upper continental crust. Geochemistry Geophysics Geosystems, 2.

Miller, C.A., Peucker-Ehrenbrink, B., Walker, B.D., Marcantonio, F., 2011. Re-assessing the surface cycling of molybdenum and rhenium. Geochimica Et Cosmochimica Acta, 75(22): 7146-7179.

Monteiro, F.M., Pancost, R.D., Ridgwell, A., Donnadieu, Y., 2012. Nutrients as the dominant control on the spread of anoxia and euxinia across the Cenomanian-Turonian oceanic anoxic event (OAE2): Model-data comparison. Paleoceanography, 27.

Morford, J.L., Emerson, S., 1999. The geochemistry of redox sensitive trace metals in sediments. Geochimica Et Cosmochimica Acta, 63(11-12): 1735-1750.

Nagler, T.F. et al., 2014. Proposal for an International Molybdenum Isotope Measurement Standard and Data Representation. Geostandards and Geoanalytical Research, 38(2): 149-151.

Nakagawa, Y, Takano, S., Firdaus., M.L., Norisuye, K., Hirata, T., Vance, D., Sohrin, Y. 2012. The molybdenum isotopic composition of the modern ocean. Geochemical Journal, 42, 2, 131-141

Neubert, N., Nagler, T.F., Bottcher, M.E., 2008. Sulfidity controls molybdenum isotope fractionation into euxinic sediments: Evidence from the modern Black Sea. Geology, 36(10): 775-778.

Noordmann, J. et al., 2015. Uranium and molybdenum isotope systematics in modern euxinic basins: Case studies from the central Baltic Sea and the Kyllaren fjord (Norway). Chemical Geology, 396: 182-195.

Ostrander, C.M., Owens, J.D., Nielsen, S.G., 2017. Constraining the rate of oceanic deoxygenation leading up to a Cretaceous Oceanic Anoxic Event (OAE-2: similar to 94 Ma). Science Advances, 3(8).

Owens, J.D., Reinhard, C.T., Rohrssen, M., Love, G.D., Lyons, T.W., 2016. Empirical links between trace metal cycling and marine microbial ecology during a large perturbation to Earth's carbon cycle. Earth and Planetary Science Letters, 449: 407-417.

Owens, J.D., Gill, B.C., Jenkyns, H.C., Bates, S.M., Severmann, S., Kuypers, M.M., Woodfine, R.G., Lyons, T.W. 2013. Sulfur isotopes track the global extend and dynamics of euxinia during Cretaceous Oceannic Anoxic Event 2. PNAS, 110, 46, 18407-18412

Pearce, C.R., Cohen, A.S., Coe, A.L., Burton, K.W., 2008. Molybdenum isotope evidence for global ocean anoxia coupled with perturbations to the carbon cycle during the early Jurassic. Geology, 36(3): 231-234.

Poulson Brucker, R.L., McManus, J., Severmann, S., Berelson, W.M., 2009. Molybdenum behavior during early diagenesis: Insights from Mo isotopes. Geochemistry Geophysics Geosystems, 10: Q06010.

Poulson, R.L., Siebert, C., McManus, J., Berelson, W.M., 2006. Authigenic molybdenum isotope signatures in marine sediments. Geology, 34(8): 617-620.

Poulton, S.W., Canfield, D.E., 2011. Ferruginous Conditions: A Dominant Feature of the Ocean through Earth's History. Elements, 7(2): 107-112.

Poulton, S.W. et al., 2015. A continental-weathering control on orbitally driven redox-nutrient cycling during Cretaceous Oceanic Anoxic Event 2. Geology, 43(11): 963-966.

Raiswell, R. et al., 2018. THE IRON PALEOREDOX PROXIES: A GUIDE TO THE PITFALLS, PROBLEMS AND PROPER PRACTICE. American Journal of Science, 318(5): 491-526.

Rudnick, R.L., Gao, S., 2004. Composition of the Continental Crust. In: Holland, H.D., Turekian, K.K. (Eds.), Treatise on Geochemistry. Elsevier, Amsterdam, pp. 1-64.

Schmidtko, S., Stramma, L., Visbeck, M., 2017. Decline in global oceanic oxygen content during the past five decades. Nature, 542(7641): 335-+.

659 Scholz, F., 2018. Identifying oxygen minimum zone-type biogeochemical cycling in Earth history using
660 inorganic geochemical proxies. Earth-Science Reviews, 184: 29-45.
661 Scholz, F. et al., 2019a. Oxygen minimum zone-type biogeochemical cycling in the Cenomanian-Turonian
662 Proto-North Atlantic across Oceanic Anoxic Event 2. Earth and Planetary Science Letters, 517: 50-60.
663 Scholz, F. et al., 2019b. Shelf-to-basin iron shuttle in the Guaymas Basin, Gulf of California. Geochimica Et
664 Cosmochimica Acta, 261: 76-92.
665 Scholz, F., Siebert, C., Dale, A.W., Frank, M., 2017. Intense molybdenum accumulation in sediments
666 underneath a nitrogenous water column and implications for the reconstruction of paleo-redox
667 conditions based on molybdenum isotopes. Geochimica Et Cosmochimica Acta, 213: 400-417.
668 Schonfeld, J. et al., 2015. Records of past mid-depth ventilation: Cretaceous ocean anoxic event 2 vs. Recent
669 oxygen minimum zones. Biogeosciences, 12(4): 1169-1189.
670 Scott, C., Lyons, T.W., 2012. Contrasting molybdenum cycling and isotopic properties in euxinic versus non-
671 euxinic sediments and sedimentary rocks: Refining the paleoproxies. Chemical Geology, 324: 19-27.
672 Siebert, C., McManus, J., Bice, A., Poulson, R., Berelson, W.M., 2006. Molybdenum isotope signatures in
673 continental margin marine sediments. Earth and Planetary Science Letters, 241(3-4): 723-733.
674 Siebert, C., Nagler, T.F., Kramers, J.D., 2001. Determination of molybdenum isotope fractionation by double-
675 spike multicollector inductively coupled plasma mass spectrometry. Geochemistry Geophysics
676 Geosystems, 2: art. no.-2000GC000124.
677 Siebert, C., Nagler, T.F., von Blanckenburg, F., Kramers, J.D., 2003. Molybdenum isotope records as a
678 potential new proxy for paleoceanography. Earth and Planetary Science Letters, 211(1-2): 159-171.
679 Trabucho-Alexandre, J. et al., 2010. The mid-Cretaceous North Atlantic nutrient trap: Black shales and OAEs.
680 Paleoceanography, 25.
681 Tribovillard, N., Algeo, T.J., Lyons, T., Riboulleau, A., 2006. Trace metals as paleoredox and
682 paleoproductivity proxies: An update. Chemical Geology, 232(1-2): 12-32.
683 Wasylenki, L.E. et al., 2011. The molecular mechanism of Mo isotope fractionation during adsorption to
684 birnessite. Geochimica Et Cosmochimica Acta, 75(17): 5019-5031.
685 Westermann, S., Vance, D., Cameron, V., Archer, C., Robinson, S.A., 2014. Heterogeneous oxygenation states
686 in the Atlantic and Tethys oceans during Oceanic Anoxic Event 2. Earth and Planetary Science
687 Letters, 404: 178-189.
688 Zheng, Y., Anderson, R.F., van Geen, A., Kuwabara, J., 2000. Authigenic molybdenum formation in marine
689 sediments: A link to pore water sulfide in the Santa Barbara Basin. Geochimica Et Cosmochimica
690 Acta, 64(24): 4165-4178.
691